This article has been accepted for publication in a future issue of this journal, but has not been fully edited. Content may change prior to final publication. Citation information: DOI 10.1109/TPWRD.2015.2440446, IEEE Transactions on Power Delivery

Wide-Band Transformer Modeling Including Core Non-Linear Effects

Bjørn Gustavsen, *Fellow, IEEE*

***Abstract*—Wide-band, black-box transformer models can be obtained via frequency sweep measurements on transformer terminals followed by rational model extraction via passive curve fitting. These models do however not include core non-linearity effects. A modeling approach is introduced where a wide-band linear model is connected in parallel with a non-linear 50/60 Hz model using filters. The filters are used to ensure a smooth transition from the 50/60 Hz model to the wide-band model with increasing frequency. Model stability is ensured by enforcing passivity for all possible states defined by a piecewise-linear representation of the magnetizing inductance. This hybrid modeling approach is demonstrated for the modeling of a single-phase transformer representing the alpha-mode of a three-phase two-winding transformer. The model is shown to correctly reproduce inrush currents and short circuit currents predicted by the 50/60 Hz model, and high-frequency transferred voltages predicted by the wide-band model.**

***Index Terms*—Transformer, wide-band, non-linear, simulation, transients.**

I. Introduction

TRANSFORMER high-frequency models are needed in transient overvoltage studies involving transformer network interactions as well as transfer of overvoltages between windings [1-2]. High-frequency models are routinely developed by the manufacturers starting from detailed design information and used for predicting internal winding overvoltages during the lightning impulse test [3-6]. These *white-box* models are usually unavailable to external parties and they often lack in accuracy for use in general network studies. When the model is intended for network studies only, a more practical approach is to characterize the transformer terminal behavior using frequency sweep measurements followed by model extraction via curve fitting [7-10]. The latter *black-box* model often gives highly accurate results when used in studies of high-frequency transients although the information about internal voltages is lost.

One difficulty with the black-box modeling approach is that the accuracy often deteriorates at low frequencies due to limitations in the measurement setups. The accuracy at 50/60 Hz is often important as it may impact the initial conditions prior to the high-frequency transient event, e.g. in the case of a through-fed fault [11]. As a remedy, it was proposed in [12] to merge the wide-band data with those generated by a standard 50/60 Hz model prior to model extraction via curve fitting. However, this alternative model is still limited as it is not capable of taking into account core non-linear effects [13]. It is known that the non-linear *B-H* characteristics of the steel results in a shift in frequency and magnitude of the impedance frequency responses up to several tens of kHz, depending on the transformer terminal conditions [14], [15]. These changes in frequency response characteristics may substantially impact the conditions prior to a fast transient event, e.g. the transformer inrush current preceding a circuit breaker operation or fault, or the magnetizing current when disconnecting an unloaded transformer.

One way of combining non-linear and frequency-dependent effects in the same model was introduced in [16] where a non-linear core model was connected to a winding model which accounts for frequency-dependent eddy current losses in windings. The difficulty in determining the parameters of the winding model was addressed in [17] which made use of measured *R*/*L* characteristics. Still, this modeling approach remains limited in frequency range up to the transformer first resonance frequency as it does not include the transformer internal capacitance effects.

This paper introduces an alternative way of combining transformer non-linear and frequency-dependent effects which permits to include the transformer's high-frequency resonances. This capability is achieved by modifying the merging procedure in [12] to also include core non-linear effects. A filtered wide-band model is connected in parallel with a filtered 50/60 Hz model that allows to connect non-linear branch elements to internal nodes. The combined model is subjected to passivity enforcement with respect to the external terminals so that the model is passive, for any combination of incremental inductances defined by a piecewise-linear representation of the non-linear magnetizing inductances. The approach is demonstrated for the α-mode of a three-phase two-winding transformer that is modeled by a *T*-type equivalent circuit. The non-linear magnetizing inductance is represented by a two-segment piecewise-linear inductance.

Manuscript received Jan. 22, 2015.

B. Gustavsen is with SINTEF Energy Research, N-7465 Trondheim, Norway (e-mail: bjorn.gustavsen@sintef.no).

This work was supported by the Norwegian Research Council (RENERGI Programme) with additional support from DONG Energy, EdF, EirGrid, Hafslund Nett, National Grid, Nexans Norway, RTE, Siemens Wind Power, Statnett, and Statkraft.

This article has been accepted for publication in a future issue of this journal, but has not been fully edited. Content may change prior to final publication. Citation information: DOI 10.1109/TPWRD.2015.2440446, IEEE Transactions on Power Delivery

II. Hybrid Modeling Procedure

A. Transformer Data

We assume that a set of small-signal measurements have been performed which characterizes the transformer external behavior by its terminal admittance matrix $\mathbf{Y}_{wb}(\omega)$ with respect to its external terminals,

$$\mathbf{i}(\omega) = \mathbf{Y}_{wb}(\omega)\mathbf{v}(\omega) \tag{1}$$

We further assume that a 50/60 Hz model is available from which wide-band admittance samples $\mathbf{Y}_{50}(\omega)$ can be calculated for a given value of the magnetizing inductance L_m,

$$\mathbf{i}(\omega) = \mathbf{Y}_{50}(L_m;\omega)\mathbf{v}(\omega) \tag{2}$$

We will in this work assume a *T* equivalent circuit representation of a single-phase transformer with the magnetizing inductance represented by a piecewise-linear inductance, see Fig. 1. The short-circuit impedance is split equally between the high-voltage and low-voltage side, giving an admittance $\mathbf{Y}_{50,sc}(\omega)$ on both sides.

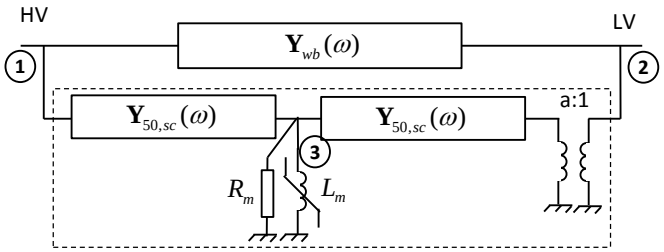

Fig. 1. Topology and data input for single-phase hybrid transformer model.

B. Filtering

The objective is to calculate a total model which is dominated by the behavior defined by the 50/60 Hz data at low frequencies and by that of the wide-band data at high frequencies. This is achieved by respectively multiplying $\mathbf{Y}_{wb}(\omega)$ and $\mathbf{Y}_{50,sc}(\omega)$ by high-pass and low-pass filters [12] (Fig. 2),

$$\tilde{\mathbf{Y}}_{wb}(\omega) = h_{HP}(\omega)\mathbf{Y}_{wb}(\omega) \tag{3a}$$

$$\tilde{\mathbf{Y}}_{50,sc}(\omega) = h_{LP}(\omega)\mathbf{Y}_{50,sc}(\omega) \tag{3b}$$

where

$$h_{HP}(\omega) = \frac{j\omega}{j\omega + \omega_{HP}} \tag{4a}$$

$$h_{LP}(\omega) = \frac{\omega_{LP}}{j\omega + \omega_{LP}} \tag{4b}$$

One will ideally choose $\omega_{HP}=\omega_{LP}$; however it will be shown that allowing different values may significantly reduce the passivity violations that need to be removed.

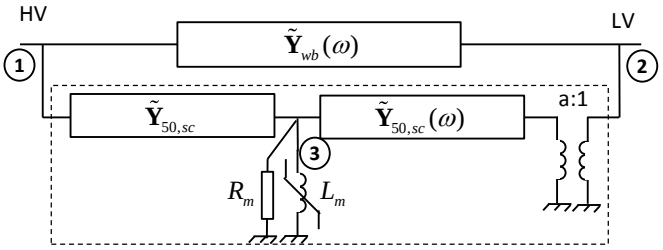

Fig. 2. Filtering of responses.

C. Model Extraction

The filtered wide-band response $\tilde{\mathbf{Y}}_{wb}(\omega)$ is fitted with a pole-residue type rational model [18-20],

$$\tilde{\mathbf{Y}}_{wb}(\omega) \cong \mathbf{Y}_1(\omega) = \mathbf{R}_{1,0} + \sum_{i=1}^{N_1} \frac{\mathbf{R}_{1,i}}{j\omega - a_{1,i}} \tag{5}$$

Further, a three-terminal admittance model $\tilde{\mathbf{Y}}_2(\omega)$ for the 50 Hz part within the dashed box in Fig. 2 is calculated using nodal analysis, excluding the magnetizing inductance. The three-port model is fitted with a pole-residue type rational model,

$$\tilde{\mathbf{Y}}_2(\omega) \cong \mathbf{Y}_2(\omega) = \mathbf{R}_{2,0} + \sum_{i=1}^{N_2} \frac{\mathbf{R}_{2,i}}{j\omega - a_{2,i}} \tag{6}$$

The accuracy of the approximation (6) is close to machine precision since the underlying model of the data is rational. The resulting model structure is shown in Fig. 3.

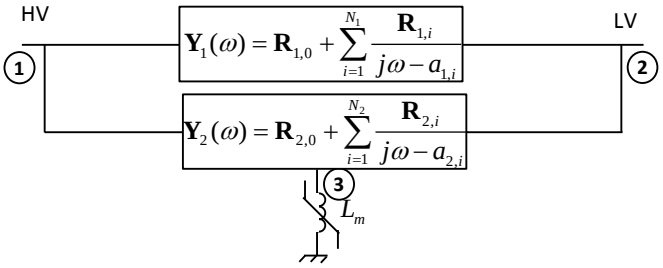

Fig. 3. Pole-residue model representation.

D. Passivity Enforcement

The total model is required to be passive seen from the external terminals 1 and 2, for any of the N_{seg} incremental inductances defined by the piecewise-linear inductance. This is achieved by perturbing the residues of $\mathbf{Y}_1$,

$$\Delta\mathbf{Y}_1(\omega) = \Delta\mathbf{R}_{1,0} + \sum_{i=1}^{N_1} \frac{\Delta\mathbf{R}_{1,i}}{j\omega - a_{1,i}} \tag{7}$$

such that the *total* model seen from terminals 1 and 2 becomes passive. To achieve this, the 50/60 Hz model with its associated non-linear inductance is first converted into a set of N_{seg} two-terminal models where each model includes one linear segment $L_{m,j}$ and has node 3 eliminated (see resulting model in Fig. 4),

This article has been accepted for publication in a future issue of this journal, but has not been fully edited. Content may change prior to final publication. Citation information: DOI 10.1109/TPWRD.2015.2440446, IEEE Transactions on Power Delivery

$$\mathbf{Y}_3(L_{m,j};\omega) = \mathbf{R}_{3,0}(L_{m,j}) + \sum_{i=1}^{N_2} \frac{\mathbf{R}_{3,i}(L_{m,j})}{j\omega - a_{3,i}(L_{m,j})},\ j = 1\ldots N_{seg} \quad (8)$$

This gives a set of N_{seg} total models

$$\mathbf{Y}_{tot}(L_{m,j};\omega) = \mathbf{Y}_1(\omega) + \mathbf{Y}_3(L_{m,j};\omega) \quad (9)$$

and it is required that the perturbed, total model

$$\mathbf{Y}_{tot}(L_{m,j};\omega) + \Delta\mathbf{Y}_1(\omega) \quad (10)$$

is passive for all segments *j*, i.e. the real part of the perturbed (symmetrical) model is positive definite,

$$\mathbf{G}(\omega) = \mathrm{Re}\{\mathbf{Y}_{tot}(L_{m,j};\omega) + \Delta\mathbf{Y}_1(\omega)\} > 0\ \forall\omega,\ j = 1\ldots N_{seg} \quad (11)$$

The passivity condition (11) is enforced using the residue perturbation method in [21] which is based on the eigenvalue perturbation theorem. Usage of [21] gives the constrained least squares problem

$$\min_{\Delta\mathbf{x}} \|\mathbf{A}\| \Delta\mathbf{x} \quad s.t. \quad \mathbf{B}\Delta\mathbf{x} < \mathbf{c} \quad (12)$$

where the entries of **c** contain the required eigenvalue perturbations. The solution

$$\Delta\mathbf{x} = vec(\mathbf{R}_i^1; i = 0,\ldots, N_1) \quad (13)$$

defines via (7) the sought perturbation

$$vec(\Delta\mathbf{Y}_1) = \mathbf{M}\Delta\mathbf{x} \quad (14)$$

The constraint part of (12) is applied at a set of frequencies where passivity violations are present while the least squares part of (12) ensures that the perturbation $\Delta\mathbf{Y}_1$ is minimal, with appropriate weighting. In this work, inverse magnitude weighting with respect to $\mathbf{Y}_{tot}$ is used, evaluated at the first (linear) segment. Details about the calculation of **A**, **B** and **c** is found in [21]. The passivity correction scheme using (12) and (10) is solved repeatedly until all passivity violations have been removed. The passivity violations are in this process detected using a half-size test matrix which is computed directly from the rational model of $\mathbf{Y}_{tot}$ in (9) [22].

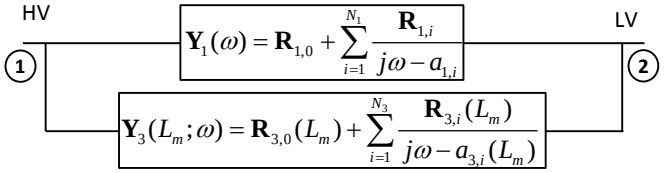

Fig. 4. Pole-residue model representation embedding the piecewise-linear inductance.

E. Model for Time Domain Simulation

Following the passivity enforcement of $\mathbf{Y}_1$, the model in Fig. 3 is ready for time domain simulation. For use in EMTP-type simulation environments, the two pole-residue models can be included via recursive convolution [23],[24] or via a lumped equivalent circuit [7],[25]. The piecewise-linear inductance is implemented directly using the native piecewise-linear component available in the simulation tool.

III. Data Case

The proposed modeling procedure is in its presented form applicable for the modeling of single-phase transformers. Since such transformer was not available to the author, a three-phase transformer was used for generating a suitable data set.

The transformer data set is the one presented in [12] of a 300 kVA distribution transformer with U_{np}=11.430 kV and U_{ns}=0.235 kV. The transformer short-circuit data is shown in Table I along with the voltage ratio. The non-linear magnetizing inductance is modeled by two linear segments as shown in Table II (assumed values) which respectively represent the behavior in the linear region and in heavy saturation. The segments are described in terms of the (λ, i) curve (peak value) and the associated incremental inductance values L_m. The knee point corresponds exactly to operation at nominal voltage and frequency. It is further assumed a large value for the magnetizing resistance, R_m=100 MΩ.

TABLE I.
SHORT-CIRCUIT PARAMETERS REF. HV SIDE, VOLTAGE RATIO.

	R_k	L_k	$a=U_{pn}/U_{sn}$
Pos. seq.	4.35 Ω	0.0564 H	48.6

TABLE II.
MAGNETIZING CHARACTERISTICS REF. HV SIDE.

Segment	λ [kVs]	i [A]	L_m [H]
1 (knee point)	29.7064	1.0724	27.7
2	30.9952	10.7243	0.1128

The 6×6 data set is replaced with a 2×2 set associated with the α-mode of the Clarke transformation **T**.

$$\begin{bmatrix} i_1 \\ i_2 \\ i_3 \end{bmatrix} = \mathbf{T}\begin{bmatrix} i_0 \\ i_\alpha \\ i_\beta \end{bmatrix},\ \begin{bmatrix} v_1 \\ v_2 \\ v_3 \end{bmatrix} = \mathbf{T}\begin{bmatrix} v_0 \\ v_\alpha \\ v_\beta \end{bmatrix} \quad (15)$$

where

$$\mathbf{T} = \begin{bmatrix} 1 & \sqrt{2} & 0 \\ 1 & -\frac{1}{\sqrt{2}} & \frac{\sqrt{3}}{\sqrt{2}} \\ 1 & -\frac{1}{\sqrt{2}} & -\frac{\sqrt{3}}{\sqrt{2}} \end{bmatrix} \frac{1}{\sqrt{3}} \quad (16)$$

We note that **T** is both real and orthogonal; hence it preserves the realness, passivity and symmetry of the original data.

The transformation is applied to each of the four sub blocks of $\mathbf{Y}_{wb}$,

$$\begin{bmatrix} \mathbf{i}_H \\ \mathbf{i}_L \end{bmatrix} = \begin{bmatrix} \mathbf{Y}_{HH} & \mathbf{Y}_{HL} \\ \mathbf{Y}_{LH} & \mathbf{Y}_{LL} \end{bmatrix} \cdot \begin{bmatrix} \mathbf{v}_H \\ \mathbf{v}_L \end{bmatrix} \quad (17)$$

and the α-component is extracted as element (2,2) of each transformed (sub) matrix. The four α-components define a single-phase transformer with components

This article has been accepted for publication in a future issue of this journal, but has not been fully edited. Content may change prior to final publication. Citation information: DOI 10.1109/TPWRD.2015.2440446, IEEE Transactions on Power Delivery

$$\mathbf{Y}_{wb,\alpha} = \begin{bmatrix} Y_{HH,\alpha} & Y_{HL,\alpha} \\ Y_{LH,\alpha} & Y_{LL,\alpha} \end{bmatrix} \tag{18}$$

The α-component $\mathbf{Y}_{50,\alpha}$ of the 50/60 Hz admittance model $\mathbf{Y}_{50}$ is equal to the positive sequence admittance component when the transformer admittance submatrices are assumed to be balanced.

Fig. 5 shows the four elements of $\mathbf{Y}_{wb,\alpha}$ and $\mathbf{Y}_{50,\alpha}$ after eliminating node 3 of $\mathbf{Y}_{50,\alpha}$ under the assumption that node 3 is open. It is observed that the admittance elements of $\mathbf{Y}_{wb,\alpha}$ and $\mathbf{Y}_{50}$ are similar in magnitude around 3-5 kHz. In the remaining work subscript α is left out to simplify notation.

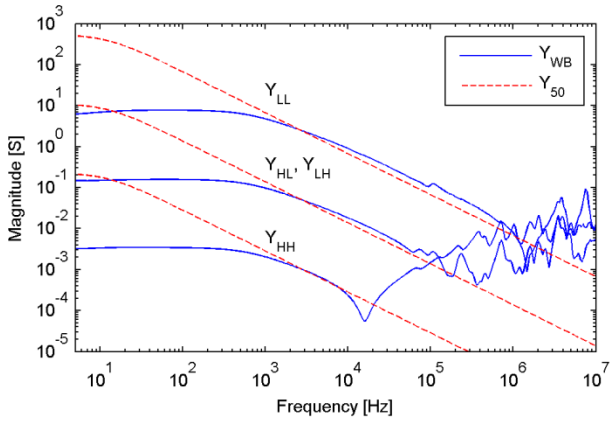

Fig. 5. α-components of $\mathbf{Y}_{wb}$ and $\mathbf{Y}_{50}$. L_m=0.

IV. Modeling

A. Filtering

The filter frequencies ω_{HP} and ω_{LP} are chosen by shifting their values while assessing the passivity violations in the raw data samples $\mathbf{Y}_{tot,raw}(L_{m,j};\omega)$. This implies checking the eigenvalues of $(\mathbf{Y}_{tot,raw}+\mathbf{Y}_{tot,raw}^{H})/2$ over the available frequency samples. Fig. 6 shows the maximum passivity violation as a function of the filter parameters. It is observed that the passivity violations are strongly reduced when choosing ω_{LP} larger than ω_{HP}. The filter parameters are accordingly chosen as shown in Table III which gives very small violations in the data. Fig. 7 shows the effect of this filtering on the admittance elements in Fig. 5. It is seen that the filtering suppresses the low-frequency behavior of $\mathbf{Y}_{wb}$ and the high-frequency behavior of $\mathbf{Y}_{50}$.

Table III.
Filter Parameters.

ω_{LP} [rad/s]	ω_{HP} [rad/s]
2π·5000	2π·1000

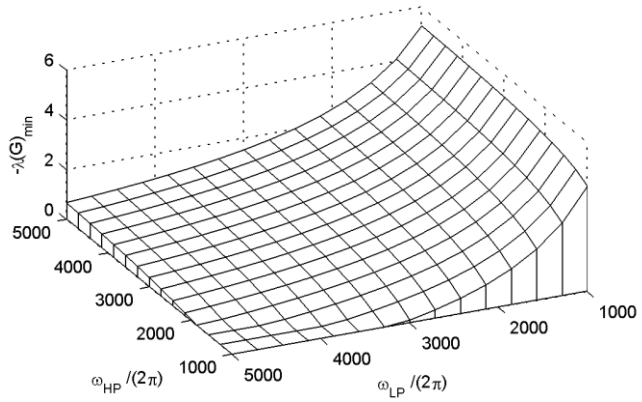

Fig. 6. Maximum passivity violation in $\mathbf{Y}_{tot}(L_{m,j})$ as a function of filter parameters.

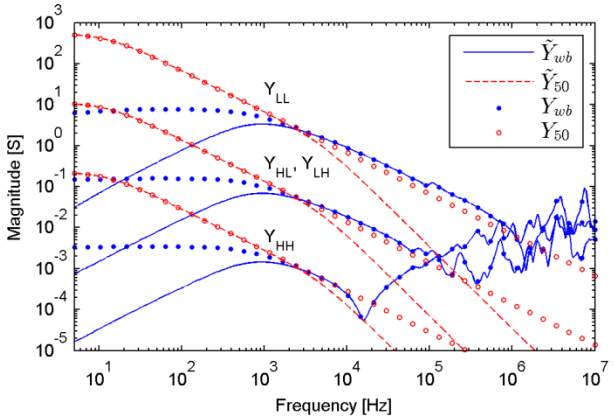

Fig. 7. Components of $\mathbf{Y}_{wb}$ and elements of $\mathbf{Y}_{50}$, after filtering.

B. Pole-Residue Fitting

The rational models $\mathbf{Y}_1(\omega)$ and $\mathbf{Y}_2(\omega)$ are calculated using vector fitting (VF) [18-20], in combination with mode-revealing transformation (MRT) [26], with N_1=40 and N_2=3. Inverse magnitude weighting is used for $\mathbf{Y}_1(\omega)$ while the fitting error results virtually zero for $\mathbf{Y}_2(\omega)$ irrespective of the weighting scheme. Fig. 8 shows the behavior of the total model $\mathbf{Y}_{tot}$ (9) with L_m=0. It is observed that as frequency increases, the behavior or the total model undergoes a smooth transition from that of the 50 Hz model to that of the wide-band model.

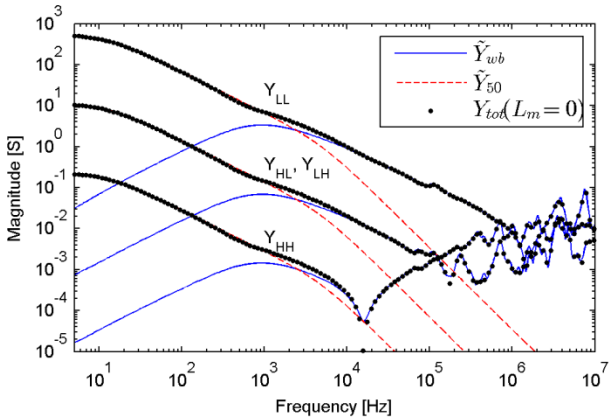

Fig. 8. Total model and filtered raw data, excluding magnetizing inductance.

This article has been accepted for publication in a future issue of this journal, but has not been fully edited. Content may change prior to final publication. Citation information: DOI 10.1109/TPWRD.2015.2440446, IEEE Transactions on Power Delivery

C. Passivity Enforcement

Passivity is next enforced by perturbing the residues of $\mathbf{Y}_1$ as described in Section II-D. Finally, the model of $\mathbf{Y}_1(\omega)$ is transformed back into the "physical domain" using the inverse MRT.

Fig. 9 shows the impact of the passivity enforcement on the small eigenvalues of $\mathbf{G}(\omega)$ in (11), for the two models $\mathbf{Y}_{tot}(L_{m,j};\omega)$, $j=1,2$. It is observed that the passivity enforcement perturbs the model such that all eigenvalues become positive.

Fig. 10 shows the impact of the perturbation on the elements of the final model ($\mathbf{Y}_{tot}$), excluding the magnetizing inductance. This result corresponds to the plot in Fig. 8.

Fig. 11 shows the the impact of the perturbation on the eigenvalues of $\mathbf{Y}_{tot}$, with the two incremental inductances included. It is further seen that the small eigenvalue of $\mathbf{Y}_{50}$ is strongly dependent on the non-linear inductance value.

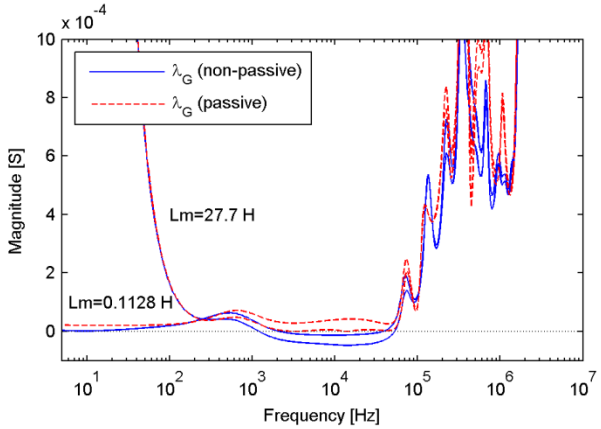

Fig. 9. Passivity enforcement. Small eigenvalue of **G**, for total model with segment 1 (L_m=27.7 H) and segment 2 (L_m=0.1128 H).

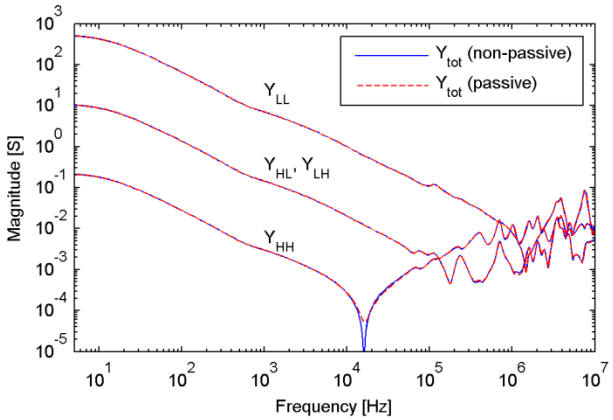

Fig. 10. Elements of the final model $\mathbf{Y}_{tot}$ (L_m=0).

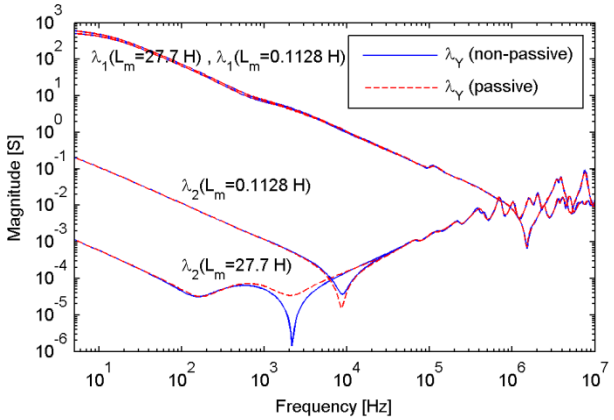

Fig. 11. Passivity enforcement. Eigenvalues of $\mathbf{Y}_{tot}$, for model including segment 1 (L_m=27.7 H) and segment 2 (L_m=0.1128 H).

D. Voltage Ratios

Figs. 12 and 13 show respectively the voltage ratio from high to low and from low to high. The plots include the voltage ratios as calculated from the (unfiltered) wide-band data $\mathbf{Y}_{wb}$, and from the total model $\mathbf{Y}_{tot}$ with the two alternative values for the incremental inductance L_m. It is observed that the total model gives a very good agreement with that inferred from $\mathbf{Y}_{wb}$, when L_m corresponds to the first (non-saturated) segment. This result is as expected since the frequency sweep measurements used for obtaining $\mathbf{Y}_{wb}$ are small-signal excitations. The two figures also show that the voltage ratio by the total model agrees very closely with the nominal voltage ratio, at frequencies below 30 kHz and 5 kHz, respectively.

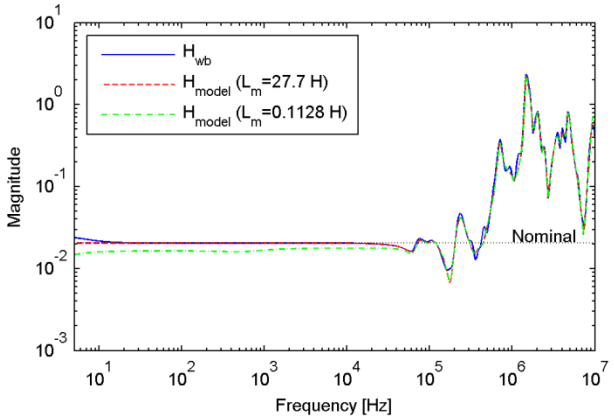

Fig. 12. Voltage transfer from HV side to LV side. Passive model.

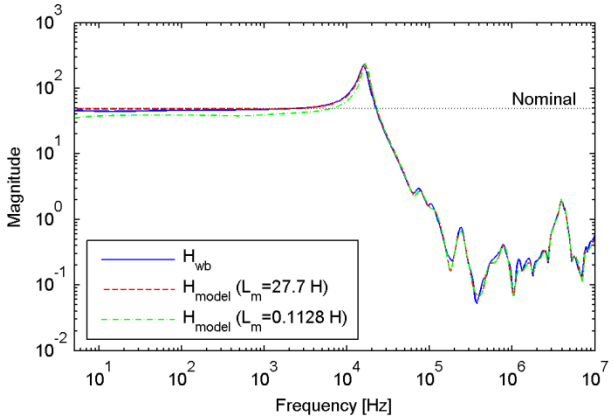

Fig. 13. Voltage transfer from LV side to HV side. Passive model.

This article has been accepted for publication in a future issue of this journal, but has not been fully edited. Content may change prior to final publication. Citation information: DOI 10.1109/TPWRD.2015.2440446, IEEE Transactions on Power Delivery

V. Time Domain Simulation

A. Test Case

We demonstrate the application of the hybrid transformer model in a time domain simulation using PSCAD. The magnetizing inductance is represented by a piecewise-linear inductance while the two rational models representing $\mathbf{Y}_1$ and $\mathbf{Y}_2$ are included via a user-defined routine (FDTE) [27]. Fig. 14 shows a situation where the transformer HV side is fed through a cable from a 50 Hz voltage source operating at the transformer nominal voltage. Initially, both switches are open. The transformer is energized by closing SW1 at t=1 ms with SW2 open and a fault occurs on the LV side at t=30 ms. SW1 attempts to open at t=55 ms and finally SW2 attempts to open at t=80 ms. The sequence of switch operations is summarized in Table IV. The switches interrupt the current when it decreases below i_{chop}=5 A. The simulation uses a small time step length Δt=0.05 μs due to short travel time of the cable.

TABLE IV.
SWITCH STATUS.

Status	SW1	SW2
t=0 (initial)	open	open
t=1 ms	close	
t=30 ms		close
t=55 ms	open	
t=80 ms		open

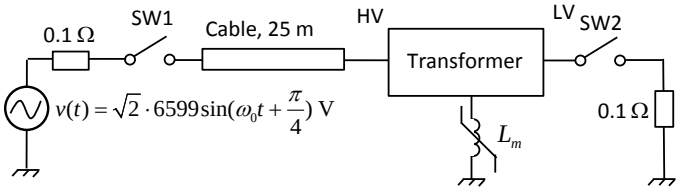

Fig. 14. Transformer energization via feeder cable, fault initiation and clearance.

The simulations are performed using three alternative models:

1. The hybrid model proposed in this work.
2. The 50 Hz model, realized by standard circuit elements including the piecewise-linear inductance branch.
3. A wide-band model obtained by fitting the original wide-band data $\mathbf{Y}_{wb}(\omega)$ with a pole-residue model.

B. Low-Frequency Currents

Fig. 15 shows the simulated current flowing through switch SW1, obtained by the proposed hybrid model, the 50 Hz model, and the wide-band model. The first two results agree very closely and show the expected half-cycle saturation current as SW1 is closed at a phase angle of 45° of the sine voltage source. The wide-band model is of course unable to include the saturation effect.

Fig. 16 shows the simulated short-circuit current through switch SW2. Again, a very good agreement is obtained between the result by the hybrid model and the 50 Hz model. The wide-band model underestimates the current as the measured short-circuit admittance is too low, see Fig. 5.

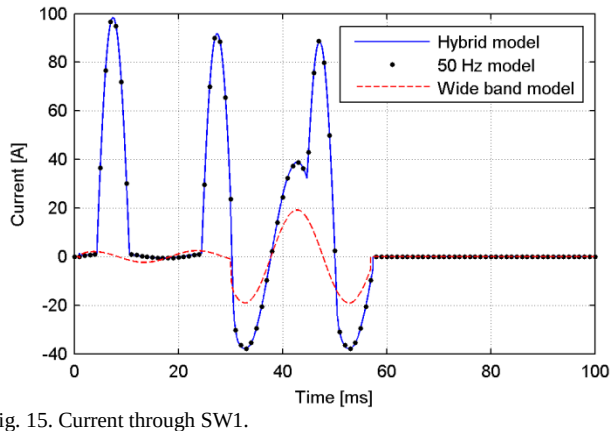

Fig. 15. Current through SW1.

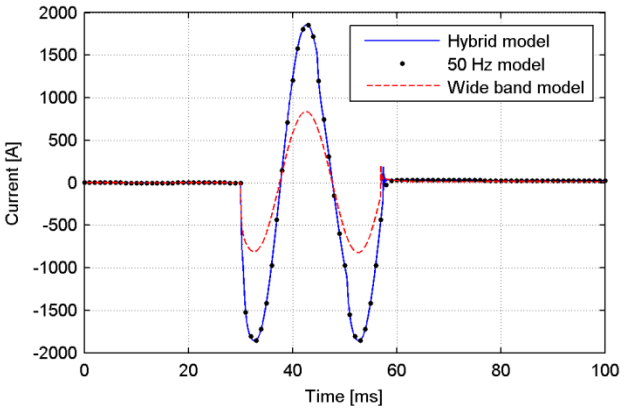

Fig. 16. Current through SW2.

C. High-Frequency Voltages

Fig. 17 shows the simulated voltage on the HV side of the transformer when SW1 closes. The closing of SW1 causes an oscillating overvoltage to result on the transformer side of the cable. This voltage waveform is very similar when calculated by the hybrid model and the wide-band model. The 50 Hz model gives a much smaller damping and a slightly higher oscillation frequency. The difference in damping can be explained by the higher input impedance of the 50 Hz model for this high frequency (~1.8 MHz) oscillation. The difference in oscillation frequency can be explained by the contribution from the terminal capacitances which are included in both the hybrid model and the wide-band model.

Fig. 18 shows the simulated voltage on the transformer LV side following the closing of the SW1. The hybrid model and the wide-band model both predict a resonant voltage buildup. The buildup occurs since the oscillation on the HV side (~1.8 MHz) coincides with a peak in the voltage transfer from the HV side to the LV side, see Fig. 12. A small deviation is seen to develop with time, due to small differences in the accuracy of the two models at high frequencies. The 50 Hz model is unable to represent this resonant condition.

This article has been accepted for publication in a future issue of this journal, but has not been fully edited. Content may change prior to final publication. Citation information: DOI 10.1109/TPWRD.2015.2440446, IEEE Transactions on Power Delivery

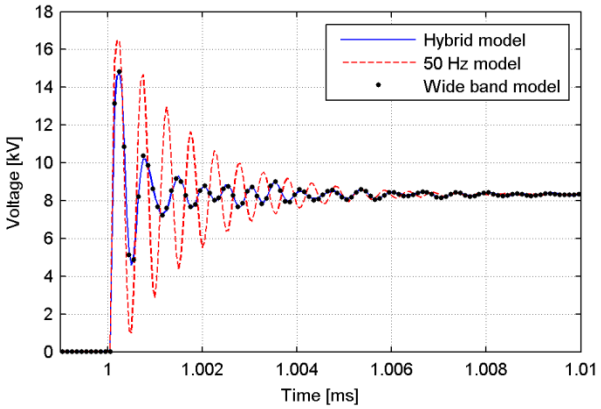

Fig. 17. Transformer HV side voltage when closing SW1.

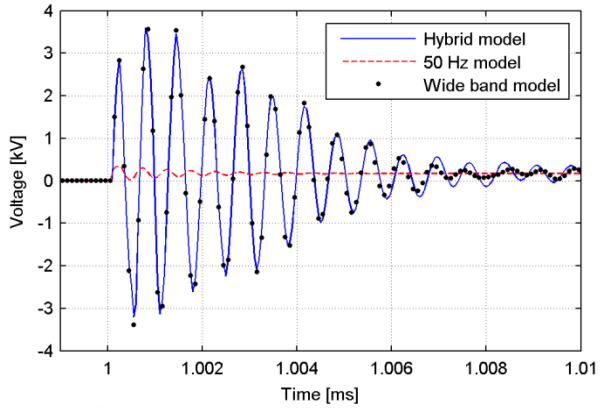

Fig. 18. Transformer LV side voltage when closing SW1.

D. Passivity

The passivity enforcement is an essential part of the modeling procedure. To see this, the cable was removed and the time step length was increased from Δt=0.05 µs to Δt=1 µs, and the simulation time was increased to 350 ms. Fig. 19 shows that the hybrid model produces an unstable result when passivity has not been enforced. The instability occurs when the current though SW2 extinguishes so that the transformer is completely disconnected from the system.

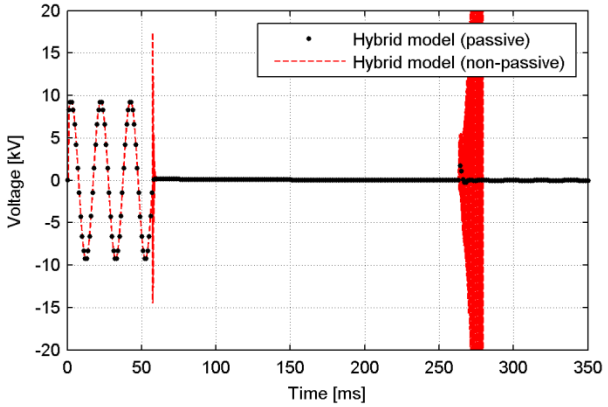

Fig. 19. Transformer voltage HV1. Impact of passivity enforcement.

VI. Discussion

A. Filter Parameters

Due to the use use of first order filters, the hybrid model undergoes with increasing frequency a smooth transition from the behavior of the 50 Hz model to that of the wide-band model. In the presented example, the filter parameters were chosen as ω_{LP}=5 kHz and ω_{HP}=1 kHz, implying that the behavior of the 50 Hz model can influence the behavior of the total model up to about 50 kHz. Still, the total model was found to reproduce the voltage ratio very accurately within the full frequency range as shown in Figs. 12 and 13. A further analysis revealed that *before* passivity enforcement, the model predicted a quite incorrect value for the dominant resonance peak in the voltage ratio from low to high, see Fig. 20. Such improvement in accuracy caused by the passivity enforcement is accidental and is not to be expected in a general case.

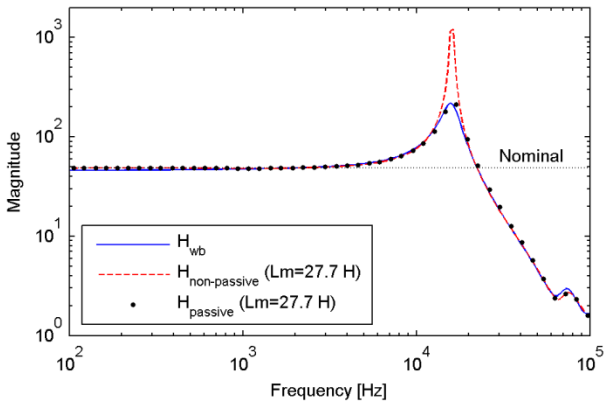

Fig. 20. Voltage transfer from LV side to HV side.

B. Model Refinement

In this work, passivity was enforced by perturbing only the parameters of $\mathbf{Y}_1$ in Fig. 3. The approach can be easily modified to also include perturbation of $\mathbf{Y}_2$. Such modification can potentially reduce the perturbation of the final model but comes at the cost of increasing the complexity of the approach.

C. Extension to Multiphase Transformers

This work considered a single phase transformer with a single piecewise-linear inductance. The example used only two linear segments but the modeling approach is general as it can in principle handle any number of segments. For use with three-phase transformers with several non-linear branches, one must require that the model remains passive for all combinations of the incremental inductances. A model with three non-linear branches having four linear segments each would thus lead to 4·4·4=64 constraints, each resulting in an augmentation of the constraint equation of (12). The increased number of constraints will necessarily lead to slower calculations.

D. Alternative Model Formulations

One obvious alternative to the proposed hybrid model is to calculate a three-terminal rational model $\hat{\mathbf{Y}}$ for the system in Fig. 2 with the non-linear inductance excluded. $\hat{\mathbf{Y}}$ can then be fitted directly with a rational model and the non-linear inductance is finally added inside the circuit simulation tool.

This approach was initially attempted; however the passivity violations were found to be more severe and harder to correct than for the hybrid model proposed in this work.

This article has been accepted for publication in a future issue of this journal, but has not been fully edited. Content may change prior to final publication. Citation information: DOI 10.1109/TPWRD.2015.2440446, IEEE Transactions on Power Delivery

This result is not surprising since passivity enforcement for the alternative three-terminal model requires the model to give stable simulations for *any* component connected to node 3, whereas the passivity enforcement of the hybrid model considers that only a finite set of inductances can be connected to node 3. Fig. 21 shows the maximum passivity violation of the raw data $\hat{\mathbf{Y}}$ for this alternative model, as a function of the filter parameters. This result corresponds directly to the result by the hybrid model in Fig. 6.

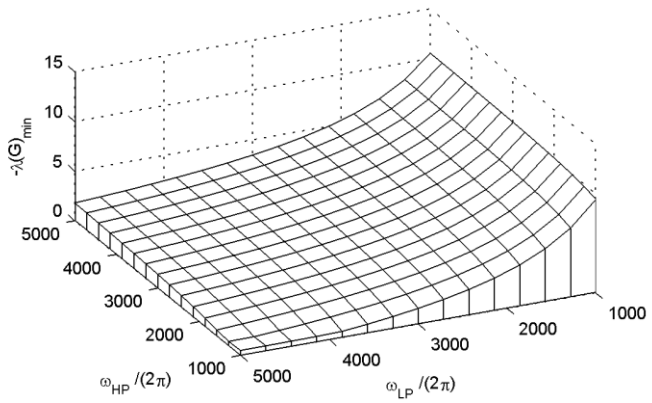

Fig. 21. Maximum passivity violation in $\hat{\mathbf{Y}}$ as a function of filter parameters.

E. Core Representations

It would also be possible to connect the magnetizing inductance to one of the external terminals, e.g. the HV terminals. This would allow to utilize the model in [12] without any further considerations to passivity. However, such an approach would give too high inrush current in deep saturation. Most models therefore include the magnetizing inductance at an internal node [13], consistently with the approach in this work.

More advanced core representations can also be used, e.g. via use of magnetic circuits and the associated topological models [28]. Here, use of a PI-circuit representation for the 50/60 Hz model can be advantageous [29].

VII. Conclusions

A hybrid model is proposed which combines data samples from a 50/60 Hz non-linear transformer model with wide-band data coming from frequency sweep measurements. The two data sets are subjected to filtering and subsequent modeling with rational functions. The total model undergoes a smooth transition from the behavior of the 50/60 Hz model at low frequencies to that of the wide-band model at high frequencies. The wide-band part of the total model is subjected to passivity enforcement so that the total model seen from external terminals is passive when a piecewise-linear inductance is connected to the star point (internal node) of the T-circuit 50/60 Hz model. Finally, the magnetizing inductance is included in the time domain simulation by connecting a piecewise-linear inductance to the internal node.

The approach is demonstrated for the α-mode of a three-phase two-winding transformer when simulating energization of a cable-fed transformer, followed by short-circuit and fault clearance. The hybrid model is found to correctly reproduce both the inrush current and the short-circuit currents as well as the high-frequency transients resulting from the energization.

VIII. References

[1] IEEE Std C57.142-2010, IEEE Guide to describe the occurrence and mitigation of switching transients induced by transformers, switching device, and system interaction.

[2] CIGRE JWG A2/C4.39, "Electrical transient interaction between transformers and the power system", Technical Report 577A/B, April 2014.

[3] W.J. McNutt, T.J. Blalock, R.A. Hinton, "Response of Transformer Windings to System Transient Voltages", *IEEE Trans. Power Apparatus and Systems*, vol. PAS-93, Issue 2, 1974, pp 457-467

[4] F. De Leon and A. Semlyen, "A complete transformer model for electromagnetic transients," *IEEE Trans. Power Delivery*, vol. 9, no. 1, pp. 231-239, Jan. 1994.

[5] E. Bjerkan and H.K. Høidalen, "High frequency FEM-based power transformer modeling: investigation of internal stresses due to network-initiated overvoltages," *Proc. Int. Conf. Power Systems Transients*, Montreal, Canada, June 19-23, 2005, 6 p.

[6] M. Popov, L. van der Sluis, R.P. Smeets, and J.L. Roldan, "Analysis of very fast transients in layer-type transformer windings", *IEEE Trans. Power Delivery*, vol. 22, no. 1, pp. 238-247, Jan 2007.

[7] A. Morched, L. Marti, and J. Ottevangers, "A high frequency transformer model for the EMTP," *IEEE Trans. Power Delivery*, vol. 8, no. 3, pp. 1615-1626, July 1993.

[8] B. Gustavsen, "Wide band modeling of power transformers", *IEEE Trans. Power Delivery*, vol. 19, no. 1, pp. 414-422, Jan. 2004.

[9] A. Borghetti, A. Morched, F. Napolitano, C.A. Nucci, "Lightning-induced overvoltages transferred through distribution power transformers", *IEEE Trans. Power Delivery*, vol. 24, no. 1, pp. 360-372, Jan. 2009.

[10] A. Holdyk, B. Gustavsen, I. Arana, J. Holboell, "Wide band modeling of power transformers using commercial sFRA equipment", *IEEE Trans. Power Delivery*, vol. 29, no. 3, pp. 1446-1453, June 2014.

[11] B. Badrzadeh and B. Gustavsen, "High-frequency modeling and simulation of wind turbine transformer with doubly-fed asynchronous generator", *IEEE Trans. Power Delivery*, vol. 27, no. 2, pp. 746-756, April 2012.

[12] B. Gustavsen, "A filtering approach for merging transformer high-frequency models with 50/60 Hz low-frequency models", *IEEE Trans. Power Delivery*, in press.

[13] J. A. Martinez and B.A. Mork, "Transformer modeling for low- and mid-frequency transients – a review", *IEEE Trans. Power Delivery*, vol. 20, no. 2, pp. 1625-1632, April 2005

[14] M. Popov, L. van der Sluis, G.C. Paap, "Investigation of the circuit breaker reignition overvoltages caused by no-load transformer switching surges", *European Transactions on Electrical Power* (ETEP), vol.11, no.6, , pp. 413-422, November/December 2001.

[15] A. O. Soysal, "A method for wide frequency range modeling of power transformers and rotating machines", *IEEE Trans. Power Delivery*, vol. 8, no. 4, pp. 1802-1810, October 1993.

[16] F. de Leon, A. Semlyen, "Complete transformer model for electromagnetic transients", *IEEE Trans. Power Delivery*, vol. 9, no. 1, pp. 231-239, Jan. 1994.

[17] N. Chiesa, B. Gustavsen, "Frequency-dependent modeling of transformer winding impedance from $R(\omega)$/L(ω) measurements", *IEEE Trans. Power Delivery*, vol. 29, no. 3, pp. 1511-1513, June 2014.

[18] B. Gustavsen and A. Semlyen, "Rational approximation of frequency domain responses by vector fitting", *IEEE Trans. Power Delivery*, vol. 14, no. 3, pp. 1052-1061, July 1999.

[19] B. Gustavsen, "Improving the pole relocating properties of vector fitting", *IEEE Trans. Power Delivery*, vol. 21, no. 3, pp. 1587-1592, July 2006.

[20] D. Deschrijver, M. Mrozowski, T. Dhaene, and D. De Zutter, "Macromodeling of multiport systems using a fast implementation of the vector fitting method", *IEEE Microwave and Wireless Components Letters*, vol. 18, no. 6, pp. 383-385, June 2008.

[21] B. Gustavsen, and A. Semlyen, "Enforcing passivity for admittance matrices approximated by rational functions", *IEEE Trans. Power Systems*, vol. 16, no. 1, pp. 97-104, Feb. 2001.

[22] A. Semlyen and B. Gustavsen, "A half-size singularity test matrix for fast and reliable passivity assessment of rational models", *IEEE Trans. Power Delivery*, vol. 24, no. 1, pp. 345-351, Jan. 2009.

[23] A. Semlyen and A. Dabuleanu, "Fast and accurate switching transient calculations on transmission lines with ground return using recursive convolutions", *IEEE Trans. Power Apparatus and Systems*, vol. 94, pp. 561-575, March/April 1975.

[24] B. Gustavsen and H.M.J. De Silva, "Inclusion of rational models in an electromagnetic transients program – Y-parameters, Z-parameters, S-parameters, transfer functions", *IEEE Trans. Power Delivery*, vol. 28, no. 2, pp. 1164-1174, April 2013.

[25] B. Gustavsen, "Computer code for rational approximation of frequency dependent admittance matrices", *IEEE Trans. Power Delivery*, vol. 17, no. 4, pp. 1093-1098, October 2002.

[26] B. Gustavsen, "Rational modeling of multi-port systems via a symmetry and passivity preserving mode-revealing transformation", *IEEE Trans. Power Delivery*, vol. 29, no. 1, pp.199-205, February 2014.

[27] B. Gustavsen, and O. Mo, "Interfacing convolution based linear models to an electromagnetic transients program", International Conf. on Power Systems Transients (IPST), Lyon, France, June 4-7, 2007, 6p.

[28] G.R. Slemon, "Equivalent circuits for transformers and machines including non-linear effects", *Proc. IEE* – Part IV: Institution Monographs, vol. 100, no. 5, pp. 129-143, 1953.

[29] F. de Leon, A. Farazmand, P. Joseph, "Comparing T and π equivalent circuits for the calculation of transformer inrush currents", *IEEE Trans. Power Delivery*, vol. 27, no. 4, pp. 2390-2398, Oct. 2012.

IX. BIOGRAPHIES

Bjørn Gustavsen (M'94–SM'2003–F'2014) was born in Norway in 1965. He received the M.Sc. degree and the Dr.Ing. degree in Electrical Engineering from the Norwegian Institute of Technology (NTH) in Trondheim, Norway, in 1989 and 1993, respectively. Since 1994 he has been working at SINTEF Energy Research where he is currently Chief Scientist. His interests include simulation of electromagnetic transients and modeling of frequency dependent effects. He spent 1996 as a Visiting Researcher at the University of Toronto, Canada, and the summer of 1998 at the Manitoba HVDC Research Centre, Winnipeg, Canada. He was a Marie Curie Fellow at the University of Stuttgart, Germany, August 2001–August 2002. He is convenor of CIGRE JWG A2/C4.52.